

# One Stone Two Birds: Redox-Sensitive Colocalized Delivery of Cisplatin and Nitric Oxide through Cascade Reactions

Jianbing Wu, Yihui Hu, Hui Ye, Sheng Zhang, Jie Zhu, Duorui Ji, Yihua Zhang, Ya Ding,\* and Zhangjian Huang\*



Cite This: *JACS Au* 2022, 2, 2339–2351



Read Online

ACCESS |

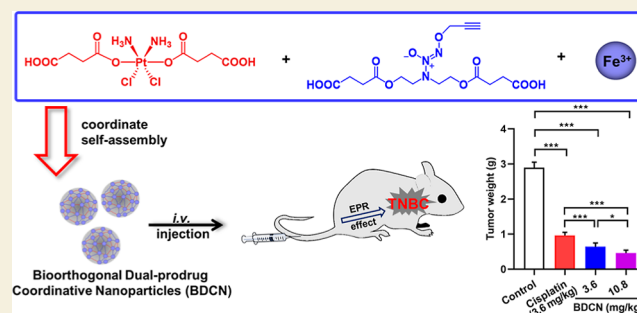
Metrics & More

Article Recommendations

Supporting Information

**ABSTRACT:** Bio-orthogonal bond-cleavage reactions have been used in cancer therapy for improving the biological specificity of prodrug activation, but the spatiotemporal consistency of reactants is still a huge challenge. Although, in most cases, the cleavage catalysts and caged prodrugs are administrated separately, it is difficult to avoid the reactions in advance before they meet at the tumor site. Herein, we design and construct novel coordinative nanoparticles, integrating two prodrugs A and B as ligands and ferric ions as coordinative centers. After nanoparticles accumulated in tumor through passive targeting, inert Pt(IV) prodrug A is specifically and spontaneously reduced into active Pt(II) cisplatin, which acts as the cleavage catalyst to subsequently initiate the *in situ* bio-orthogonal depropargylation of B, that is, O<sup>2</sup>-propargyl nitric oxide (NO) donor. The unique structure of coordinative nanoparticles ensures the spatiotemporal consistency of reactants (prodrugs A and B) and products (cytotoxic cisplatin and tumoricidal NO) for the bio-orthogonal bond-cleavage reaction, which leads to an improved synergistic therapeutic activity for triple-negative breast cancer (TNBC). This new concept of bio-orthogonal dual-prodrug coordinative nanoparticles may inspire further applications in bio-orthogonal chemistry and drug delivery for combination chemotherapy.

**KEYWORDS:** bio-orthogonal chemistry, dual-prodrug coordinative nanoparticles, platinum (IV) prodrug, nitric oxide, triple-negative breast cancer



## INTRODUCTION

Triple-negative breast cancer (TNBC) is a grievous and challenging health problem worldwide. Chemotherapies remain the backbone of current TNBC treatments in clinic.<sup>1–3</sup> However, the undesirable side effects and narrow therapeutic index are still such great concerns that limit the broad applicability of chemotherapy drugs.<sup>4</sup> These drawbacks can be reduced by the prodrug strategy to some extent. Previously established prodrug activations are based on the tumor microenvironment such as tumor redox conditions and acidity and radical oxygen species (ROS), among others. However, it is worth noting that the location targeting and reaction sensitivity of prodrug activation are still unsatisfactory.<sup>5</sup>

As an unprecedented technique to spontaneously perform specific chemical reactions and control complex cellular processes in living systems, bio-orthogonal chemistry provides handy tools for biomedicine.<sup>6</sup> It strongly supports fundamental research in the interdisciplinary fields of chemistry and biology, including biomolecule labeling,<sup>7,8</sup> chemoproteomics,<sup>9</sup> and prodrug discovery.<sup>10</sup> Particularly, bio-orthogonal bond-cleavage reactions have been successfully employed to develop selective prodrug activation in the arena of cancer therapy.<sup>11,12</sup> Different from the endogenous stimulus, bio-orthogonal

catalysts are unique and specific that facilitate bond cleavage reactions and liberation of active drugs only at the location of catalysts without interfering other biological processes.<sup>11,13,14</sup> Receptor-mediated tumor targeting of click-reaction,<sup>15</sup> enzyme-triggered bio-orthogonal reaction,<sup>16</sup> exosome-directed catalyst prodrug therapy,<sup>17</sup> enrichment-triggered prodrug activation,<sup>18</sup> and so forth, all show higher biological efficiency, specificity, and anti-interference ability. Nevertheless, strategies of prodrug activation *via* bio-orthogonal chemistry have their own pitfalls. The cleavage catalysts and caged prodrugs of current tactics are subjected to separate administration, in which the different pharmacokinetic behaviors and tissue distributions of these two substances could greatly influence the final outcomes. Despite this, the reactions between cleavage catalysts and caged prodrugs still lack location control in the tumor site, hence causing inevitable toxicity *in vivo*.<sup>12,19</sup>

Received: July 8, 2022

Revised: September 22, 2022

Accepted: September 23, 2022

Published: October 5, 2022



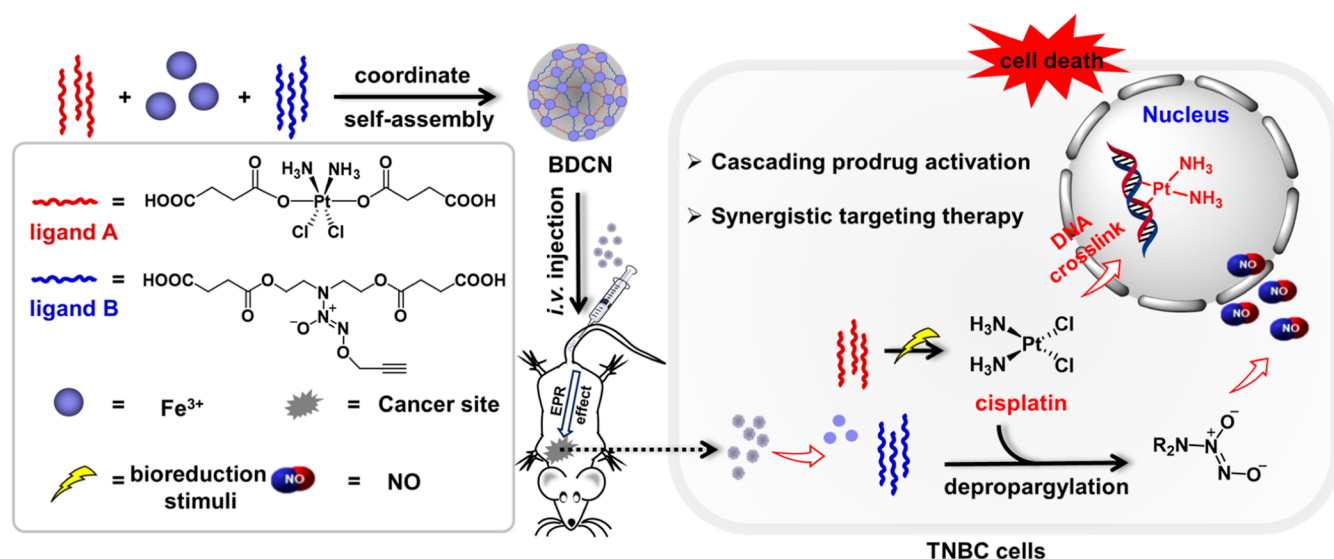


**Figure 1.** Schematic illustration for the construction of integrated BDCNs and their therapeutic mechanism of tumor-specific initiating cascade reactions.

Additionally, the cleavage catalysts usually have no pharmacological contribution, greatly reducing the atomic economy of the therapeutic system.<sup>20</sup>

Nitric oxide (NO) is known as a “star” gaseous signaling molecule that plays important roles in various biological processes *in vivo*.<sup>21</sup> It has been well-documented that high levels ( $\mu\text{M}$  to  $\text{mM}$ ) of NO could exert the promising cancer cell growth inhibitory effect *via* multiple routes. Recently, we have reported a nanoscale coordination polymer (NCP) employing the iron ion as coordinative centers to connect the nitric oxide (NO) donor (BPDB) as the polydentate bridge ligand.<sup>22</sup> This NCP is able to accumulate in tumor *via* the enhanced permeability and retention (EPR) effect and release the hydroxyl radical *via* ferrous ion-mediated Fenton reaction and NO under the trigger of glutathione (GSH). This is a typical *in situ* prodrug activation based on the tumor microenvironment, that is, high levels of GSH. The uniqueness of the NCP is that metal nodes, ferrous ions, exert their contribution to produce hydroxyl radicals for synergizing the tumoricidal effect of NO. In fact, many of other transition metals are also used to catalyze bio-orthogonal bond-cleavage reactions.<sup>11,12</sup> However, for constructing prodrug-based coordinative nanoparticles using metals with bio-orthogonal catalytic activity, there is one huge challenge that must be overcome. It is that how to mask the catalytic activity of metals under normal physiological conditions and recover their prodrug activation abilities once reaching the tumor site. Thus, we set out to find the right metal to achieve this goal.

Pt(II) drugs, such as cisplatin, are extensively involved in treating a variety of cancers, but their uses are limited because of toxicities. Pt(IV) complexes, as kinetically inert platinum prodrugs, have higher stability and less side effects than Pt(II) compounds.<sup>23</sup> A series of NCPs bearing *c,c,t*-(diamminedichlorodisuccinato) Pt(IV) (DSCP, a prodrug of cisplatin) as bridging ligands have been developed.<sup>24–26</sup> These NCPs are capable of delivering DSCP specifically into the tumor site, and then, DSCP is reduced to Pt(II) cisplatin under the redox environment, exerting promising tumoricidal activity with desirable safety. Interestingly, we found that Pt(II), but not Pt(IV), is able to catalyze a bio-orthogonal bond-cleavage

reaction, that is, depropargylation reaction.<sup>27</sup> Thus, this catalytic selectivity based on the element valence conversion of Pt(IV)/Pt(II) may open a new door for the construction of bio-orthogonal coordinative nanoparticles.

Inspired by these findings, we propose a new concept of integrated bio-orthogonal dual-prodrug coordinative nanoparticles (BDCNs) for antitumor prodrug activation for the first time. As shown in Figure 1, Pt(IV) compound (A), a prodrug of cisplatin bearing two terminal carboxyl groups, and NO prodrug *O*<sup>2</sup>-propargyl diazeniumdiolate B with two terminal carboxyl groups and the *O*<sup>2</sup>-propargyl moiety are used as bridging ligands, and ferric ions act as coordinative centers. A, B, and ferric ions are mixed in a certain ratio to form BDCNs, which contains two elements of bio-orthogonal chemistry, masked trigger (A) and caged active group (B). It is hypothesized that BDCNs may be stable during circulation, and once reaching tumor tissues, inert Pt(IV) compound A can be reduced to catalytically active Pt(II) cisplatin in cancer cells, and the latter triggers depropargylation of prodrug B to generate high levels of NO. Together with the DNA cross-linking effect of cisplatin, the synergistic effect of NO produces potent anticancer activity. This BDCN system possesses the following fascinating features: (1) the proportion of two prodrugs can be flexibly adjusted as needed; (2) the cascade reactions specifically initiated at the tumor site can both exert synergistic anticancer activity and reduce side effects; (3) the integration of the catalyst and reactant in one system not only avoids the pharmacokinetic complexity of separated administration but also enhances the efficiency of bio-orthogonal reactions, which improves the potential for clinical translation. Importantly, the idea of integrating two prodrugs into one NCP and achieving synergistic activities *via* cascade reactions under a specific microenvironment can be flexibly extended to other drug delivery/design strategies for combination chemotherapy.

## RESULTS AND DISCUSSION

### Synthesis of Ligands for BDCNs

The synthetic routes of ligands A and B in BDCNs are depicted in Scheme S1. Briefly, cisplatin A-1 was oxidized to

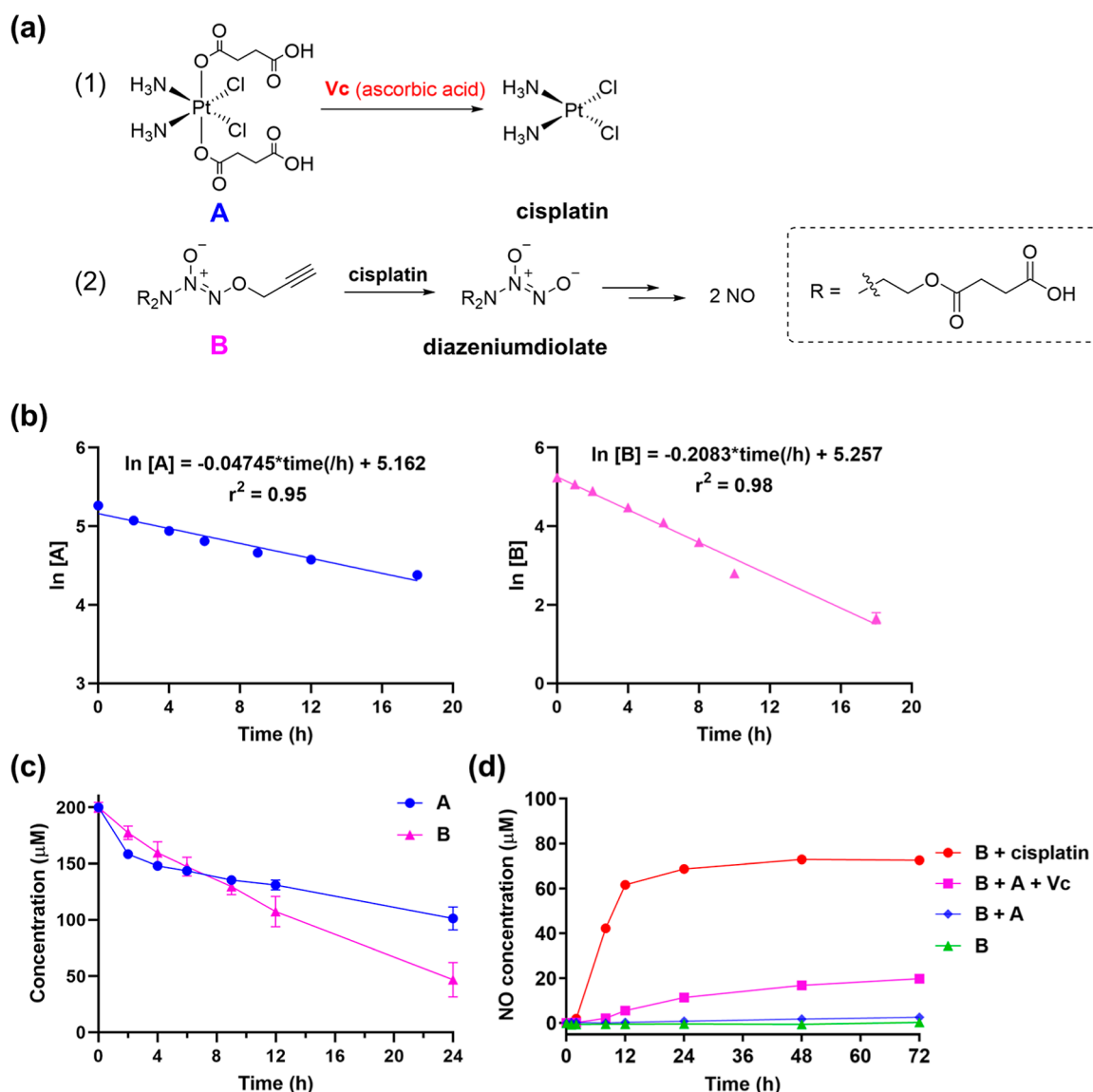


**Figure 2.** Bio-orthogonal chemistry reaction occurred within ligands A (via a reduction by Vc) and B. (a) Activation routes for the bio-orthogonal chemistry reaction. (b) Decomposition kinetics behaviors and rates of A and B in the presence of Vc and cisplatin, respectively, and the kinetic reaction equations were calculated. (c) Decomposition curve of A (200  $\mu\text{M}$ ) and B (200  $\mu\text{M}$ ) in the presence of Vc (1 mM) (monitored by HPLC). (d) NO releasing from B (100  $\mu\text{M}$ ) under different conditions (A, 200  $\mu\text{M}$ ; cisplatin, 200  $\mu\text{M}$ ; and Vc, 200  $\mu\text{M}$ ). Data are expressed as mean  $\pm$  SD ( $n = 3$ ).

Pt(IV) A-2, which was subsequently treated with succinic anhydride to furnish Pt(IV) ligand A with dicarboxylic acid groups.<sup>28</sup> Besides, the reaction of NO gas (50 psi) with diethanolamine (B-1) in the presence of NaOMe in anhydrous methanol/ether offers sodium diazeniumdiolate B-2, which was further reacted with propargyl bromide to produce  $O^2$ -propargyl diazeniumdiolate B-3. Then, B-3 was reacted with succinic anhydride in the presence of DMAP to give ligand B bearing dicarboxylic acid groups. Additionally, we synthesized two similar ligands A' and B' for negative BDCN controls. As shown in Scheme S1, the oxidized cisplatin moiety in A was replaced by hydroquinone to offer A', which has no catalytic activity, and the  $O^2$ -propargyl group in B was replaced by the  $O^2$ -propyl group to give B', in which  $O^2$ -propyl cannot be decayed by Pt(II). Synthetic procedures and characteristic data of all organic ligands are presented in the Supporting Information.

### Cascade Bio-orthogonal Reactions

We first investigated the bio-orthogonal cleavage reaction between ligands A and B in the cell-free system. Based on our assumption, compound A can be reduced by cytoplasmic reductants such as L-ascorbic acid ( $\text{H}_2\text{Asc}$ , Vc)<sup>29–31</sup> to form cisplatin, which subsequently triggers the cleavage of  $O^2$ -propargyl in B to liberate the diazeniumdiolate free anion, spontaneously releasing two molecules of NO (see the equations in Figure 2a). To verify this process, the reduction of prodrug A in the presence of Vc (1 mM) in aqueous solution (pH = 3.66) and the depropargylation reaction of B with the existence of cisplatin in aqueous solution were detected by the high-performance liquid chromatography (HPLC) method. As shown in Figures S1a and 2b, compound A was reduced in the presence of Vc, and the decomposition kinetics parameters were calculated with a pseudo-first-order kinetics  $K = 0.04745 \pm 0.0026 \text{ h}^{-1}$  and a half-life of  $14.60 \pm$

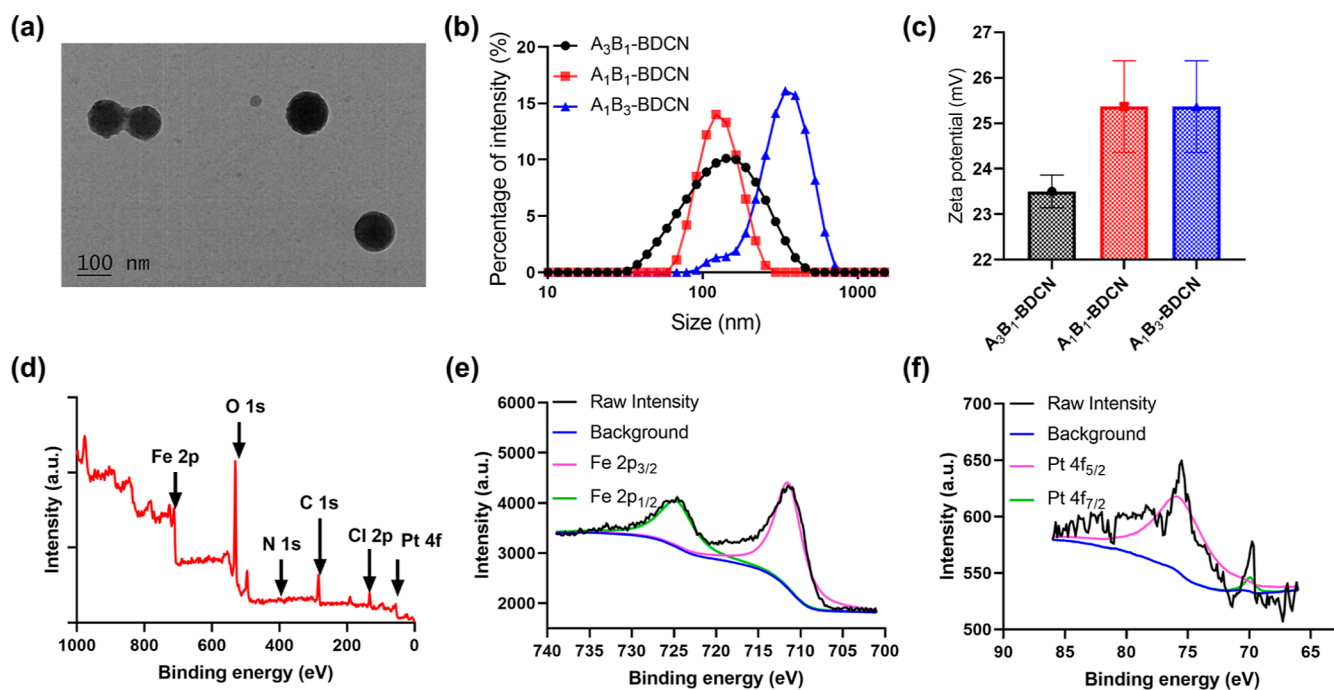


**Figure 3.** Characterization of  $A_1B_1$ -BDCN. (a) TEM micrograph for the as-synthesized  $A_1B_1$ -BDCN showing a spherical nanostructure (scale bar = 100 nm). (b) Hydrodynamic diameters (size: nm) for the as-synthesized BDCNs measured by dynamic light scattering (DLS). (c) Zeta potential for the as-synthesized BDCNs. Data are expressed as mean  $\pm$  SD ( $n = 3$ ). (d) X-ray photoelectron full spectroscopy for  $A_1B_1$ -BDCN. (e) XPS Fe spectrum for  $A_1B_1$ -BDCN. (f) XPS Pt spectrum for  $A_1B_1$ -BDCN.

0.80 h. Meanwhile, compound **B** was gradually reduced with the existence of cisplatin (Figures S1b and 2b), and the pseudo-first-order kinetics  $K$  and half-life were  $0.2083 \pm 0.0063 \text{ h}^{-1}$  and  $3.33 \pm 0.10 \text{ h}$ , respectively. Interestingly, the decomposition of **A** in the presence of **Vc** under physiological conditions (PBS, pH = 7.4, 37 °C) was slowed down (Figure S1c,d), suggesting that the acidic tumor microenvironment could be favorable for **Vc**-induced reduction. After incubating the mixture of **A** and **B** in the presence of **Vc**, we observed the decomposition of **A** followed by **B** in a time-dependent manner (Figure 2c). The NO-releasing behaviors were detected by Griess assay.<sup>32</sup> As shown in Figure 2d, both compound **B** alone and the combination of **A** with **B** were stable in PBS (pH = 7.4, 37 °C) without NO releasing within 72 h. In sharp contrast, both **B** plus molar equivalent cisplatin and **B** plus equivalent **A** in the presence of equivalent **Vc** generated NO in a time-dependent manner. In sum, these data preliminarily revealed the proposed cascade reduction and bio-orthogonal activation reactions between **A** and **B** in the presence of **Vc** in cell-free systems.

### Preparation and Characteristic of BDCNs

Subsequently, we used prodrugs **A** and **B** as ligands and ferric ions as coordinative centers to construct the BDCNs. Briefly, the ligands **A** and **B** were dissolved in aqueous sodium bicarbonate solution; then, the two solutions were mixed, and an aqueous solution of ferric trichloride hexahydrate was added. The obtained mixture was stirred, and the BDCN was purified by dialysis (details in the Supporting Information). Keeping the number of ferric ions constant and excess, we first studied the influence of the molar ratio of **A** and **B** ( $A/B/Fe^{3+} = 3:1:3$ ,  $1:1:3$ , and  $1:3:3$ ) on the BDCN morphology. As shown in Figures 3a,b and S2a, only an equal molar ratio of **A** and **B** reacting with threefold ferric ions produced spherical nanoparticles with a proper diameter of *ca.* 100 nm. Thus, we

chose the BDCN with an equal molar ratio of **A** and **B** (named  $A_1B_1$ -BDCN) for further study. The optimized  $A_1B_1$ -BDCN also showed a relatively stable positive potential at  $25.37 \pm 1.01 \text{ mV}$  (Figure 3c). Then, the composition of  $A_1B_1$ -BDCN was determined by X-ray photoelectron spectroscopy (XPS), demonstrating that C, N, O, Fe, and Pt are the main constituents in the  $A_1B_1$ -BDCN skeleton (Figure 3d). Additionally, the XPS spectra of Fe (2p) and Pt (4f) were analyzed using XPS Peak 4.0 software. As shown in Figure 3e,f, the XPS spectral regions were mainly of  $Fe^{3+}$  ions and Pt (4f) of  $Pt^{4+}$  ions. Moreover, the actual composition ratio of each ligand and coordinative ferric ions in  $A_1B_1$ -BDCN was determined and calculated by measuring the remaining **A**, **B**, and  $Fe^{3+}$  in the reaction supernatant using the HPLC (for **A** and **B**) or colorimetric (for  $Fe^{3+}$ ) method (Table S1). It was calculated that the ratio of  $A/B/Fe^{3+}$  in the case of  $A_1B_1$ -BDCN was 1:1.2:6.02, which was nearly consistent with theoretical values of  $A/B$ . Moreover, we measured the ratio of representative element hydrogen in  $A_1B_1$ -BDCN by elemental analysis (EA) to calculate the ratio of **A** and **B**. The results showed that the hydrogen content was 4.25%, so the ratio of  $A/B$  was determined to be 1:1.23, which was consistent with the result obtained from the HPLC method mentioned above.

In addition, we synthesized other BDCNs including  $A'_1B_1$ -,  $A_1B'_1$ -, and  $A'_1B'_1$ -BDCN as bio-orthogonal negative controls for comparison, and the characterizations are shown in Figure S2a–c. It was found that the as-synthesized  $A'_1B_1$ -,  $A_1B'_1$ -, and  $A'_1B'_1$ -BDCN did not possess spherical nanostructures with appropriate dimension, which may influence EPR effects and cellular penetrability.<sup>33–35</sup>

### Cascade Activation of BDCNs in Cancer Cells

We then verified the bio-orthogonal characteristics and antiproliferative effects of BDCNs in cancer cells. As shown in Figure 4a, incubation of  $A_1B_1$ -BDCN with a low level of **Vc**

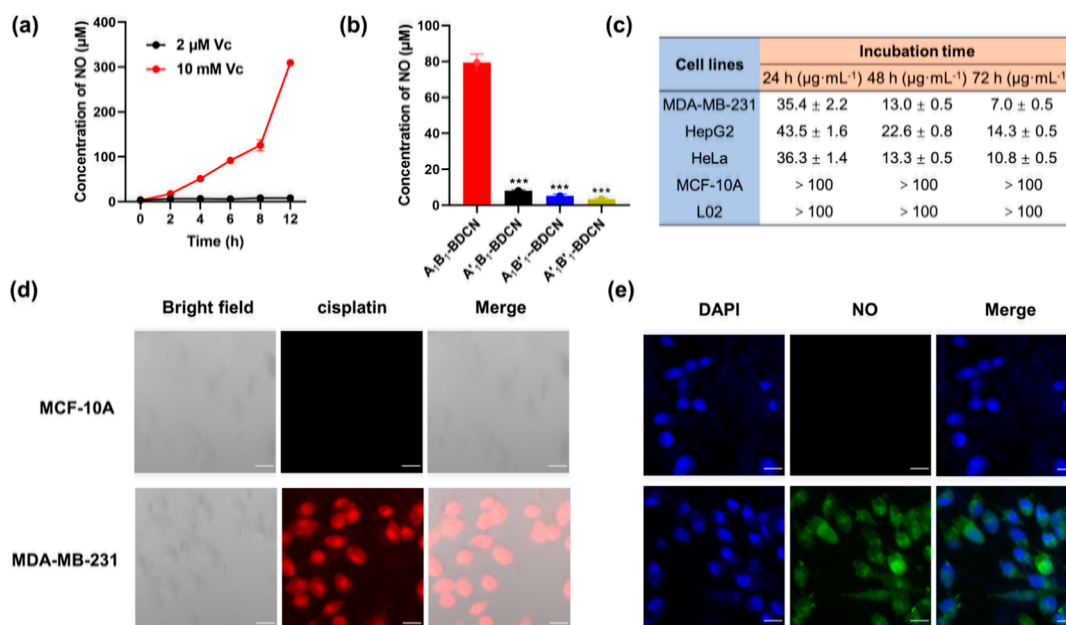


**Figure 4.** Bio-orthogonal reaction of A<sub>1</sub>B<sub>1</sub>-BDCN *in vitro*. (a) NO releasing from A<sub>1</sub>B<sub>1</sub>-BDCN (200 µg/mL) in the presence of Vc at different concentrations. (b) NO releasing from A<sub>1</sub>B<sub>1</sub>-, A<sub>1</sub>B<sub>1</sub>-, A<sub>1</sub>B<sub>1</sub>- and A<sub>1</sub>B<sub>1</sub>-BDCN, (100 µg/mL) in the presence of Vc (10 mM) for 12 h. \*\*\**P* < 0.001 vs A<sub>1</sub>B<sub>1</sub>-BDCN. (c) IC<sub>50</sub> values of A<sub>1</sub>B<sub>1</sub>-BDCN against MDA-MB-231, HepG2, HeLa, MCF-10A, and L01 cells after incubation for 24, 48, or 72 h. Data are expressed as mean ± SD (*n* = 3). (d and e) Representative confocal laser scanning microscopy (CLSM) images of cisplatin generation and NO releasing of A<sub>1</sub>B<sub>1</sub>-BDCN in MCF-10A or MDA-MB-231 cells, respectively (scale bar = 20 µm).

(2 µM, simulating the normal cell microenvironment)<sup>36</sup> was unable to release NO, while treatment of high concentration of Vc (10 mM, simulating the tumor cell microenvironment)<sup>29,37</sup> significantly accelerated the generation of NO in a time-dependent manner during 0–12 h. There was little NO released from the negative controls including A<sub>1</sub>B<sub>1</sub>-, A<sub>1</sub>B<sub>1</sub>- and A<sub>1</sub>B<sub>1</sub>-BDCN even under a relatively strong reducing condition (Figure 4b). In addition, A<sub>1</sub>B<sub>1</sub>-BDCN possessed reasonable stability with very little NO releasing in various media including PBS (pH = 7.4, 6.8, or 5.4), cell culture medium RPMI-1640, DMEM, and MCF-10A specific culture medium (Figure S3a). Importantly, these BDCNs displayed no effects on the hemolysis of erythrocytes at all test concentrations (from 20 to 200 µg/mL), suggesting their good biocompatibility (Figure S3b). Accordingly, we investigated the antiproliferative activity of BDCNs against several cancer cells and normal cells by MTT assay. As shown in Figure 4c, A<sub>1</sub>B<sub>1</sub>-BDCN exhibited potent antiproliferative activity against human TNBC MDA-MB-231 cells, human hepatocarcinomatous HepG2 cells, and human breast cancer MCF-7 cells in a time-dependent manner. Among them, A<sub>1</sub>B<sub>1</sub>-BDCN had the most potent inhibitory activity against MDA-MB-231 cells with the lowest IC<sub>50</sub> value of 7.01 µg/mL after incubation for 72 h, while all of the negative controls including A<sub>1</sub>B<sub>1</sub>-, A<sub>1</sub>B<sub>1</sub>- and A<sub>1</sub>B<sub>1</sub>-BDCN in the concentration range from 5 to 200 µg/mL did not show an inhibitory effect (Figure S4). Furthermore, the <sup>195</sup>Pt cellular uptake amount of A<sub>1</sub>B<sub>1</sub>-BDCN is approximately three times that of the A<sub>1</sub>B<sub>1</sub>-BDCN group (Figure S5), which may be due to the poor penetrability of the latter caused by unsatisfied morphology, accounting for the weak antiproliferative effects. Importantly, A<sub>1</sub>B<sub>1</sub>-BDCN displayed weak activity (IC<sub>50</sub> > 100 µg/mL) against normal cells including human epithelial breast MCF-10A cells and human fetal hepatocyte L02 cells, suggesting desirable selectivity to cancer cells.

We then used a fluorescent ratiometric Pt(II) probe RDC1<sup>38</sup> and an NO probe DAF-FM DA<sup>39</sup> to investigate cisplatin and NO generation in cells, respectively. As shown in Figure 4d,e, A<sub>1</sub>B<sub>1</sub>-BDCN significantly produced cisplatin and NO in MDA-MB-231 cells, whereas little cisplatin or NO was generated in normal MCF-10A cells, indicating the TNBC selectivity of A<sub>1</sub>B<sub>1</sub>-BDCN. Additionally, little NO was generated in MDA-MB-231 cells after treatment with B, which indicated that B displayed a good stability in tumor cells (Figure S6).

These results together with the antiproliferative data mentioned above demonstrated that A<sub>1</sub>B<sub>1</sub>-BDCN is selectively reduced in cancer cells to generate the Pt(II) moiety, which initiates the O<sup>2</sup>-cleavage reaction to spontaneously release NO *in situ*, generating synergistic and potent activity against cancer cells, while sparing normal cells.

#### *In Vivo* Tumor Accumulation of BDCNs

Having proved that A<sub>1</sub>B<sub>1</sub>-BDCN can generate cisplatin and release NO at the same location and exert selective and potent antiproliferation activity against MDA-MB-231 cells, we aimed to demonstrate whether A<sub>1</sub>B<sub>1</sub>-BDCN could be exclusively activated in tumor *in vivo*. First, we encapsulated fluorescent molecule IR-780<sup>40</sup> into A<sub>1</sub>B<sub>1</sub>-BDCN to acquire IR-780@A<sub>1</sub>B<sub>1</sub>-BDCN (see the procedures in the Methods section and the characterization data in Figure S7). The tumor aggregation and organ distribution of IR-780@A<sub>1</sub>B<sub>1</sub>-BDCN were tracked through animal imaging after intravenous injection to the MDA-MB-231 subcutaneous tumor model in nude mice, and free IR-780 was used as a control. As shown in Figure 5a,b, the IR-780@A<sub>1</sub>B<sub>1</sub>-BDCN group exhibited obviously strong fluorescence in the tumor site of xenograft mice. However, the mice treated with free IR-780 did not show any fluorescence in the tumor site. Subsequently, we chose the time point at 24 h to explore the distribution of IR-780@A<sub>1</sub>B<sub>1</sub>-BDCN in tumor and other main organs in mice. As shown in Figure 5c,d, we observed that free IR-780 was mainly

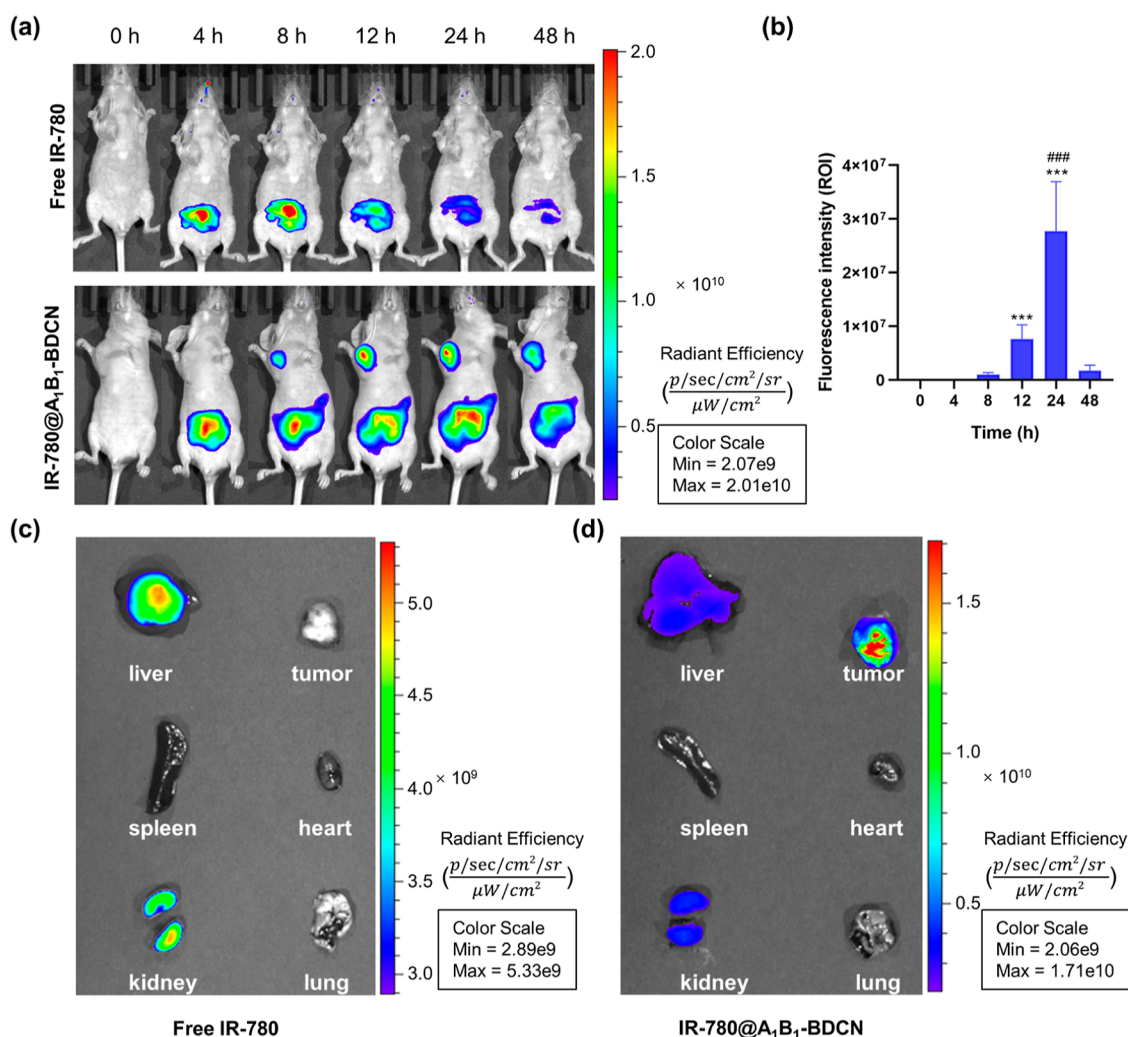


**Figure 5.** Fluorescence-guided location of A<sub>1</sub>B<sub>1</sub>-BDCN in MDA-MB-231 breast cancer xenograft mice models ( $\lambda_{\text{ex/em}} = 660/780$  nm). (a) Representative full-body fluorescence images of mice xenograft models at 0, 4, 8, 12, 24, and 48 h after *i.v.* injection with free IR-780 (0.0643 mg/kg) or IR-780@A<sub>1</sub>B<sub>1</sub>-BDCN (with equal fluorescent intensity of IR-780). (b) Quantification of fluorescence in tumor of IR-780@A<sub>1</sub>B<sub>1</sub>-BDCN group mice at different time points. Data are expressed as mean  $\pm$  SD ( $n = 8$ ). \*\*\* $P < 0.001$  vs time-point 8 h, ### $P < 0.001$  vs time-point 12 h. (c,d) *Ex vivo* fluorescence imaging of tumor and main organs removed from MDA-MB-231 breast cancer xenograft mice after 24 h post *i.v.* injection with free IR-780 (0.0643 mg/kg) or IR-780@A<sub>1</sub>B<sub>1</sub>-BDCN (with equal fluorescent intensity of IR-780).

distributed in liver and kidney tissues, but little fluorescence was observed in tumors. In contrast, IR-780@A<sub>1</sub>B<sub>1</sub>-BDCN is mainly distributed in tumor, whereas only weak fluorescence was detected in the liver and kidneys. These results intensively demonstrated that A<sub>1</sub>B<sub>1</sub>-BDCN is stable during circulation after intravenous injection and specifically accumulates in the tumor site *via* passive targeting.

#### **In Vivo Generation of Cisplatin and NO from A<sub>1</sub>B<sub>1</sub>-BDCN**

To further confirm that cisplatin and NO could release specifically in cancer cells after being delivered into the target site, we established a cancer cell-implanted zebrafish model to address this issue. In brief, the zebrafish implanted with DiD- or DiI-labeled MDA-MB-231 cells (Figure S8) were incubated with A<sub>1</sub>B<sub>1</sub>-BDCN (a final concentration of 14.4  $\mu\text{g/mL}$  and equal volume of PBS was set as the blank control) in a six-well plate at 37  $^{\circ}\text{C}$  for 24 h, followed by being collected, washed, and incubated with cisplatin probe RDC1<sup>27,38</sup> (20  $\mu\text{M}$ ) for additional 3 h or with NO probe DAF-FM DA<sup>27,39</sup> (5  $\mu\text{M}$ ) for additional 40 min. Zebrafish were subjected to CLSM or stereomicroscopy before treatment and after incubation with

the cisplatin probe/NO probe to image the location of both cancer cells and cisplatin/NO releasing (Figure 6a,d). The results showed that after incubation with A<sub>1</sub>B<sub>1</sub>-BDCN, the fluorescence location of cisplatin overlapped that of the cancer cells, and the fish treated with A<sub>1</sub>B<sub>1</sub>-BDCN exhibited significantly higher fluorescence in cancer cells than the background fluorescence in the blank control group (Figure 6b,c). Similarly, after incubation with A<sub>1</sub>B<sub>1</sub>-BDCN and followed by DAF-FM DA, as shown in the panel of merge in Figure 6e, the location of NO overlapped that of the cancer cells. The A<sub>1</sub>B<sub>1</sub>-BDCN group exhibited significantly higher fluorescence of NO in cancer cells than the blank control group (Figure 6f). Interestingly, in the backbone area of zebrafish, fluorescence of cisplatin/NO in the A<sub>1</sub>B<sub>1</sub>-BDCNs group was comparable with that in the blank control group (Figure 6c,f). These results clearly demonstrated that A<sub>1</sub>B<sub>1</sub>-BDCN could be stable *in vivo* after treatment but specifically be activated in the implanted MDA-MB-231 cells to decompose into A and B. Then, A was reduced into cisplatin *in situ*, followed by triggering the depropargylation of B,

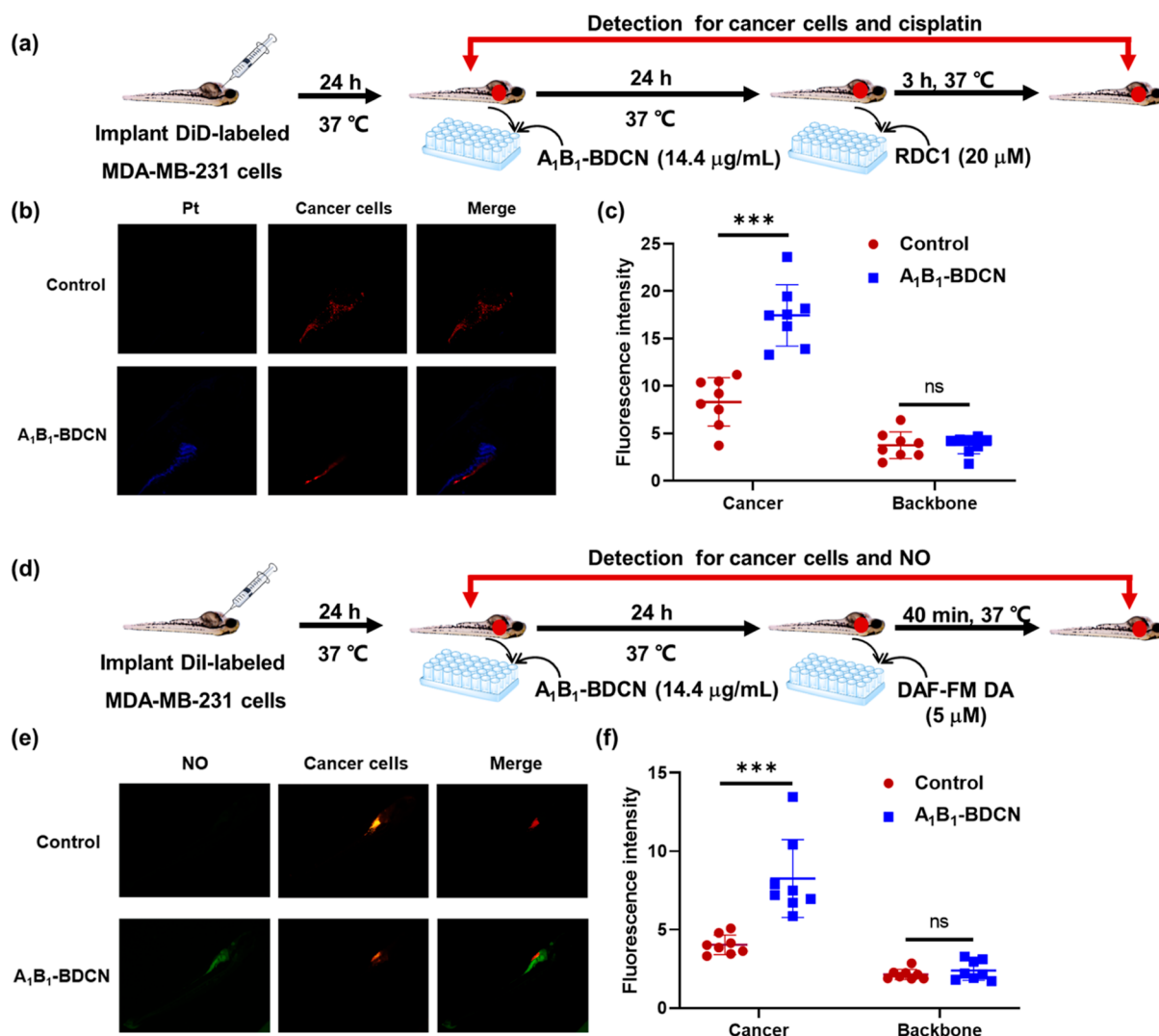


**Figure 6.** *In vivo* generation of cisplatin and NO from A<sub>1</sub>B<sub>1</sub>-BDCN. (a) Schematic illustration of the dual-imaging assay for detection of cancer cells and cisplatin. (b) Representative images of the zebrafish for each group at 3 h after the addition of RDC1 ( $\lambda_{ex/em} = 400/565$  nm, ZEN 2012 software was used to set it as blue). (c) Quantification of the fluorescent intensity in the location of the implanted cancer cells and backbone of the zebrafish at 3 h after the addition of RDC1 ( $n = 8$ ). \*\*\* $P < 0.001$  vs blank control. ns: no significance. (d) Schematic illustration of the dual-imaging assay for detection of cancer cells and NO. (e) Representative images of the zebrafish for each group at 40 min after the addition of DAF-FM DA ( $\lambda_{ex/em} = 495/515$  nm, ZEN 2012 software was used to set it as green). (f) Quantification of the fluorescent intensity in the location of the implanted cancer cell backbone of the zebrafish at 40 min after the addition of DAF-FM DA ( $n = 8$ ). \*\*\* $P < 0.001$  vs blank control. ns: no significance.

generating a large amount of NO, the latter together with cisplatin exerting potent cancer cell growth inhibitory activity *in vivo*.

#### **In Vivo Anticancer Activities of A<sub>1</sub>B<sub>1</sub>-BDCN and Biological Safety**

To evaluate the *in vivo* anticancer efficacy of A<sub>1</sub>B<sub>1</sub>-BDCN, individual nude mice were subcutaneously inoculated with MDA-MB-231 cells. After the establishment of solid tumor, the mice were randomized and treated intravenously with saline (control group) or A<sub>1</sub>B<sub>1</sub>-BDCN at different doses (*i.e.*, 0.4, 1.2, or 3.6 mg/kg) every other day for 30 consecutive days. Compared with the control group, remarkable tumor regressions were observed in all A<sub>1</sub>B<sub>1</sub>-BDCN groups in a dose-dependent manner (Figure S9). Significantly, the treatment with A<sub>1</sub>B<sub>1</sub>-BDCN at the highest test dose of 3.6 mg/kg showed 79.6% (w/w) inhibition in tumor growth (Figure S9b) and did not affect the body weights (Figure S9c) and survival

rate in mice, suggesting a good dose tolerance of A<sub>1</sub>B<sub>1</sub>-BDCN. To further explore the dose span and verify the therapeutic effect of A<sub>1</sub>B<sub>1</sub>-BDCN, the highest dose of A<sub>1</sub>B<sub>1</sub>-BDCN was increased from 3.6 to 10.8 mg/kg, using cisplatin (3.6 mg/kg) as a positive control. The results showed that A<sub>1</sub>B<sub>1</sub>-BDCN showed significant and repeatable cancer cell growth inhibitory activity (77.9% for 3.6 mg/kg dose and 84.1% for 10.8 mg/kg), which was significantly superior to that of cisplatin (66.7%, 3.6 mg/kg) (Figure 7a–d). Notably, the steady increase in mouse body weight (Figure S10) and 100% survival rate (Figure S11) of A<sub>1</sub>B<sub>1</sub>-BDCN groups indicated their excellent quality of life and biosafety. Additionally, tissue samples from all treatment groups were stained by hematoxylin and eosin (H&E). Larger area of necrosis in tumor after the treatment of BDCNs were found than those histological sections treated with cisplatin and saline treatment groups. Importantly, no obvious tissue damages were found in any of the other organs subjected to

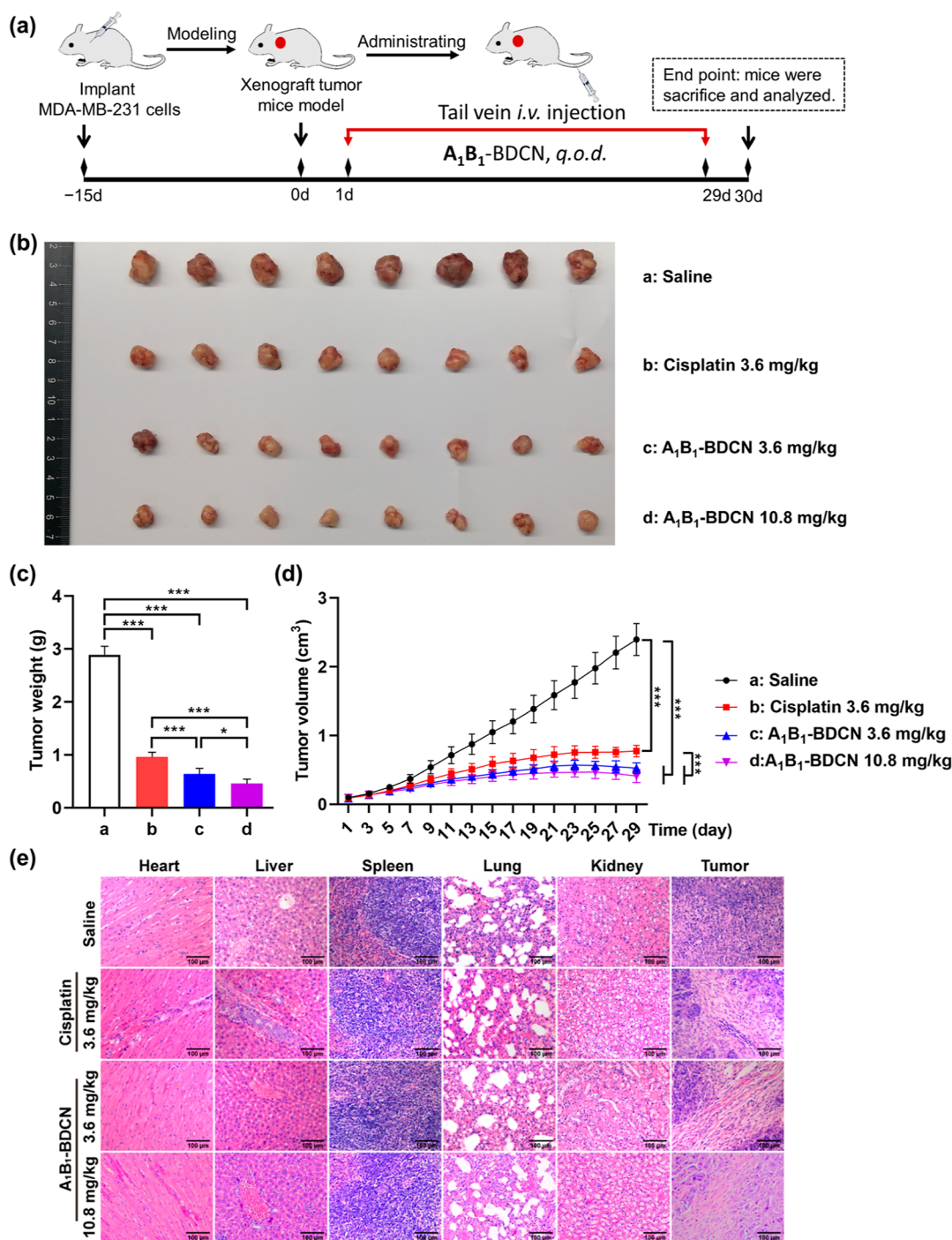


**Figure 7.** Effects of treatment with  $A_1B_1$ -BDCN on inoculated MDA-MB-231 breast cancer xenograft mice models. (a) Schematic illustration of the *in vivo* experiments. Mice were modeled and randomized into four groups and *i.v.* treated with saline (control), cisplatin, 3.6 mg/kg, and  $A_1B_1$ -BDCN (3.6 mg/kg or 10.8 mg/kg) every other day for 30 days ( $n = 8$ ). (b) Resulting tumors excised from mice of each group. (c) Tumor masses for four groups of mice, each histogram represented as mean  $\pm$  SD of eight mice. (d) Tumor volumes measured and calculated every other day. (e) H&E staining of representative tissue slices of the different treatment groups (scale bar = 100  $\mu$ m). Data are expressed as mean  $\pm$  SD from eight mice ( $n = 8$ ). \*\* $P < 0.01$  and \*\*\* $P < 0.001$ .

analysis (Figure 7e). Furthermore, we observed that *i.v.* injection with  $A_1B_1$ -BDCN (5.4 mg/kg in rats, biological equivalent dose of 10.8 mg/kg in mice) displayed no effect on the rat systemic blood pressure during a 24 h period (Figure S12). This result suggested that the  $A_1B_1$ -BDCN was stable without NO release during circulation. All these results mentioned above clearly indicated that  $A_1B_1$ -BDCN was able

to effectively inhibit the growth of MDA-MB-231 cells *in vivo* with desirable safety.

## CONCLUSIONS

TNBC is a particularly aggressive subtype of breast cancer, and cytotoxic chemotherapy will be still its backbone therapy for a long time. Herein, we propose a novel bio-orthogonal chemotherapy, integrating two prodrugs inside one coordina-

tive nanoparticle for TNBC treatment.  $A_1B_1$ -BDCN, with spherical morphology and an average size of *ca.* 100 nm, is stable during circulation without a significant effect on systemic blood pressure and efficiently enriches at tumor sites. Tumor-specific initiating cascade reactions include reduction of Pt(IV) prodrug **A** to Pt(II) by cytoplasmic reductants and the following depropargylation of NO donor **B** by Pt(II). Notably, using zebrafish models, we can clearly “see” the colocalization of cisplatin and NO selectively generated at the TNBC implanting site. Cisplatin, together with NO, produces selective, synergistic, and potent antiproliferative activity against TNBC cells. Although ferric ( $Fe^{3+}$ ) rather than ferrous ( $Fe^{2+}$ ) ions are used as coordinative centers,  $Fe^{3+}$ -initiated Fenton reactions could be much slow but can produce hydroxyl radicals to contribute tumoricidal activity.<sup>4f</sup> In the TNBC MDA-MB-231 cell xenograft mice model, in the dose range from 0.4 to 10.8 mg/kg,  $A_1B_1$ -BDCN exhibits more significant therapeutic potential and better tolerance than other controls. Furthermore, slight changes in body weights, 100% survival rate, and little damage to normal tissue are found in  $A_1B_1$ -BDCN-treated mice. These results demonstrate that  $A_1B_1$ -BDCN could be a promising chemotherapeutic agent against TNBC warranting further investigations. Basically, integration of the cleavage reagent and caged prodrug for bio-orthogonal chemistry in coordinative nanoparticles may address the application shortcomings of current bio-orthogonal chemistry, especially the separated administration and targeting ability. All in all, the novel integrated BDCN strategy may broaden the further research and potential application in bio-orthogonal chemistry and drug delivery for combination chemotherapy.

## METHODS

### General Chemistry

All reagents and solvents were bought from commercial suppliers and used as received without further drying or purification. NO gas was purchased from TIANZE GAS Co., Ltd (Nanjing, China). Melting points were determined on a MelTEMP II melting point apparatus without correction. <sup>1</sup>H NMR and <sup>13</sup>C spectra were recorded with a Bruker Avance 300 MHz spectrometer at 303 K using TMS as an internal standard. Mass spectra were recorded on a Mariner mass spectrum (ESI), and high-resolution mass spectrometry (HRMS) was recorded on an Agilent Technologies LC/MSD TOF. Analytical and preparative TLC was performed on silica gel (200–300 mesh) GF/UV 254 plates, and the chromatograms were visualized under UV light at 254 and 365 nm. Analytical reversed-phase HPLC (RPLC) was conducted on a Shimadzu Prominence HPLC system using the Innovai ODS-2 column (5  $\mu$ m, 100  $\text{\AA}$ , 150 or 250 mm  $\times$  4.60 mm). The purity of all target compounds was determined by HPLC (Shimadzu LC-20A HPLC system consisting of LC-20AT pumps and an SPD-20AV UV detector), and the compounds with a purity of >95% were used for the following experiments. All solvents were of reagent grade and, when necessary, were purified and dried by standard methods. Solutions after reactions and extractions were concentrated using a rotary evaporator operating at a reduced pressure of *ca.* 20 Torr. Compounds **A-2**,<sup>42A</sup>,<sup>24</sup> and **B-2**<sup>43</sup> were synthesized as previously described. The synthetic routes of ligands for BDCNs are depicted in Scheme S1 (Supporting Information).

### Synthesis of B-3

To a solution of diethanolamine diazeniumdiolates sodium salts (200 mg, 1.1 mmol, 1.0 equiv) in DMF (5 mL) at 0 °C under a steady stream of nitrogen was added 3-bromopropyne (84  $\mu$ L, 1.1 mmol, 1.0 equiv) in DMF (1 mL) dropwise. The mixture was allowed to warm to room temperature and stirred overnight. Then, the solvent was removed using an evaporator, and the obtained residue was treated

with H<sub>2</sub>O (20 mL) and extracted with EA (3  $\times$  50 mL). The organic layers were combined and washed with brine (20 mL), dried over Na<sub>2</sub>SO<sub>4</sub>, and evaporated under vacuum. The crude product was purified by flash chromatography on silica gel using EA and hexane for elution to give compound **B-3** as yellowish liquid (140 mg, 64.5%). <sup>1</sup>H NMR (300 MHz, Chloroform-*d*):  $\delta$  4.78 (d, *J* = 2.5 Hz, 2H), 3.74 (t, *J* = 6.9 Hz, 4H), 3.52 (s, 2H), 3.46 (t, *J* = 6.9 Hz, 4H), 2.59 (t, *J* = 2.4 Hz, 1H). <sup>13</sup>C NMR (75 MHz, chloroform-*d*):  $\delta$  77.54, 76.48, 60.99, 59.44, 56.31. MS (ESI) *m/z*: C<sub>7</sub>H<sub>13</sub>N<sub>3</sub>O<sub>4</sub> [M + Na]<sup>+</sup>, 226.0.

### Synthesis of B

To a solution of **B-3** (200 mg, 0.984 mmol, 1.0 equiv) in anhydrous THF (10 mL) was added 4-dimethylaminopyridine (12.0 mg, 0.0984 mmol, 0.1 equiv), and the mixture was allowed to stir at room temperature for 15 min. A solution of anhydrous THF (5 mL) containing succinic anhydride (200 mg, 2 mmol, 2.0 equiv) was added dropwise to the reaction mixture, and the obtained mixture was allowed to reflux overnight. After the reaction, solid residues were removed by filtration, and the filtrate was concentrated under vacuum. Then, the crude product was purified by flash chromatography on silica gel using EA and hexane for elution to give compound **B** as colorless or yellowish liquid (265 mg, 66.8%). <sup>1</sup>H NMR (300 MHz, chloroform-*d*):  $\delta$  10.21 (s, 2H), 4.75 (d, *J* = 2.4 Hz, 2H), 4.24 (t, *J* = 5.2 Hz, 4H), 3.56 (t, *J* = 5.2 Hz, 4H), 2.69–2.55 (m, 9H). <sup>13</sup>C NMR (75 MHz, chloroform-*d*):  $\delta$  177.14, 171.49, 77.03, 76.12, 61.03, 60.56, 51.70, 28.28, 28.25. ESI-HRMS *m/z* calcd for C<sub>15</sub>H<sub>21</sub>N<sub>3</sub>O<sub>10</sub> [M + H]<sup>+</sup>, 404.12997; found, 404.12965, ppm error –0.8.

### Synthesis of A'

To a solution of hydroquinone (1 g, 9.08 mmol, 1.0 equiv) in 5 mL of DMF was added succinic anhydride (3.63 g, 36.33 mmol, 4.0 equiv) and aluminum trichloride (48 mg, 0.36 mmol, 0.04 equiv), and the mixture was allowed to stir at 110 °C overnight. Then, DMF was removed by rotary evaporation. The crude product was purified by flash chromatography on silica gel using dichloromethane and methanol for elution to give compound **A'** as a white solid (305 mg, 10.8%). mp 102.5–103.7 °C. <sup>1</sup>H NMR (300 MHz, methanol-*d*<sub>4</sub>):  $\delta$  7.14 (s, 4H), 2.86 (t, *J* = 6.2 Hz, 4H), 2.72 (t, *J* = 6.3 Hz, 4H). <sup>13</sup>C NMR (75 MHz, methanol-*d*<sub>4</sub>):  $\delta$  174.41, 171.51, 148.30, 122.15, 28.77, 28.35. MS (ESI) *m/z*: C<sub>14</sub>H<sub>14</sub>O<sub>8</sub> [M + Na]<sup>+</sup>, 333.1.

### Synthesis of B'-3

To a solution of diethanolamine diazeniumdiolate sodium salts (200 mg, 1.1 mmol, 1.0 equiv) in 5 mL of DMF at 0 °C under a steady stream of nitrogen was added dropwise 1-iodopropane (187 mg, 1.1 mmol, 1.0 equiv) in 1 mL of DMF. The mixture was allowed to warm to room temperature and stirred overnight. Then, the solvent was removed using an evaporator, and the obtained residue was treated with H<sub>2</sub>O (20 mL) and extracted with EA (3  $\times$  50 mL). The organic layers were combined and washed with brine (20 mL), dried over Na<sub>2</sub>SO<sub>4</sub>, and evaporated under vacuum. The crude product was purified by flash chromatography on silica gel using EA and hexane for elution to give compound **B'-3** as yellowish liquid (151 mg, 68.2%). <sup>1</sup>H NMR (300 MHz, chloroform-*d*):  $\delta$  4.19 (t, *J* = 6.9 Hz, 2H), 3.71 (t, *J* = 6.9 Hz, 4H), 3.38 (t, *J* = 6.9 Hz, 4H), 1.83–1.68 (m, 2H), 0.96 (t, *J* = 7.4 Hz, 3H). <sup>13</sup>C NMR (75 MHz, chloroform-*d*):  $\delta$  75.80, 59.31, 56.51, 22.16, 9.92. MS (ESI) *m/z*: C<sub>7</sub>H<sub>17</sub>N<sub>3</sub>O<sub>4</sub> [M + Na]<sup>+</sup>, 230.1.

### Synthesis of B'

To a solution of **B'-3** (200 mg, 0.965 mmol, 1.0 equiv) in 10 mL of anhydrous THF was added 4-dimethylaminopyridine (11.8 mg, 0.0965 mmol, 0.1 equiv), and the obtained mixture was allowed to stir at room temperature for 15 min. A solution of 5 mL of anhydrous THF containing succinic anhydride (200 mg, 2 mmol, 2.1 equiv) was added dropwise to the reaction mixture, and the obtained mixture was allowed to reflux overnight. After the reaction, solid residues were removed by filtration, and the filtrate was concentrated under vacuum. Then, the crude product was purified by flash chromatography on silica gel using EA and hexane for elution to give compound **B'** as colorless or yellowish liquid (280 mg, 71.2%). <sup>1</sup>H NMR (300 MHz,

chloroform-*d*):  $\delta$  10.19 (s, 2H), 4.21–4.04 (m, 6H), 3.42 (t,  $J = 5.3$  Hz, 4H), 2.62–2.50 (m, 8H), 1.75–1.59 (m, 2H), 0.87 (t,  $J = 7.5$ , 1.8 Hz, 3H).  $^{13}\text{C}$  NMR (75 MHz, chloroform-*d*):  $\delta$  177.36, 171.93, 75.72, 61.46, 52.40, 28.70, 28.67, 22.06, 9.90. ESI-HRMS  $m/z$  calcd for  $\text{C}_{15}\text{H}_{25}\text{N}_3\text{O}_{10}$   $[\text{M} + \text{H}]^+$ , 408.16127; found, 408.16148, ppm error 0.5.

### Preparation of BDCNs

A (1 mL, 10 mM, dissolved in 20 mM  $\text{NaHCO}_3$ ) and 1 mL of 10 mM B (dissolved in 20 mM  $\text{NaHCO}_3$ ) were mixed and stirred for 10 min at r.t.; then, 1 mL of 60 mM  $\text{FeCl}_3 \cdot 6\text{H}_2\text{O}$  (dissolved in water) was added and stirred for another 6 h away from light. Using the UF membrane with a molecular weight cutoff 5000 dialyzed overnight in pure water,  $\text{A}_1\text{B}_1$ -BDCN aqueous solution was obtained. Other proportions of BDCNs can be provided by adjusting the adding ratio of A and B. Lyophilization of the aqueous solution offered the corresponding solid state of BDCNs. Additionally,  $\text{A}'_1\text{B}'_1$ ,  $\text{A}'_1\text{B}'_1$ , and  $\text{A}_1\text{B}'_1$ -BDCN were synthesized by the same method as that of  $\text{A}_1\text{B}_1$ -BDCN.

### Determination of the Actual Composition Ratio of Each Ligand and Coordinative Ferric Ions in BDCNs

Briefly, according to the abovementioned protocol for the synthesis of BDCN, aqueous  $\text{NaHCO}_3$  solutions of ligands A and B were mixed, followed by adding ferric chloride aqueous solution. After the reaction, the resultant  $\text{A}_1\text{B}_1$ -BDCN aqueous solution was centrifuged to obtain the supernatant and precipitate. Then, a part of the supernatant was taken for HPLC analysis to determine the concentrations of ligand A and B in it. Also, the content of ferrous ions was determined by the colorimetric method. We can obtain the concentration of each component in the  $\text{A}_1\text{B}_1$ -BDCN by calculating according to the abovementioned results and the feeding concentration of ligands and ferrous ions before reaction. On the other hand, the content of the hydrogen element was determined to be 4.25% using an elemental analyzer. As the theoretical hydrogen content of A and B is 3.02 and 5.25%, respectively, the ratio of the ligand was calculated to be 1:1.23 by solving the equations accordingly.

### Preparation of IR-780@ $\text{A}_1\text{B}_1$ -BDCN

The IR-780@ $\text{A}_1\text{B}_1$ -BDCN aqueous solution was obtained by adding 2.4 mL of 1 mM IR-780 into  $\text{A}_1\text{B}_1$ -BDCN aqueous solution, followed by stirring at r.t. overnight and dialyzing with the UF membrane to wipe off the unloaded IR-780. The load efficiency was examined and calculated by the fluorescence of IR-780@ $\text{A}_1\text{B}_1$ -BDCN and that of free IR-780.

### Pt(II) Release Measurement *In Vitro* Using the RDC1 Probe

RDC1 was synthesized according to previously reported procedures and used as a fluorescent indicator of Pt(II).<sup>38</sup> When cells grown in a 96-well plate reached 80% confluence, they were washed with PBS. The test compound was incubated with MCF-10A or MDA-MB-231 cells for 3 h. The cells were washed and resuspended with RDC1 (20  $\mu\text{M}$ ) for another 4 h. Pt(II) generation was measured with the CLSM with excitation and emission wavelengths of 400 and 565 nm, respectively.

### NO Release Measurement *In Vitro* Using the DAF-FM DA Probe

DAF-FM DA (Beyotime, Nanjing, China) was used as a fluorescent indicator of intracellular NO.<sup>39</sup> When cells grown in a 96-well plate reached 80% confluence, they were washed with PBS. After being loaded with 5  $\mu\text{M}$  DAF-FM DA at 37 °C for 20 min, the cells were rinsed three times with PBS and incubated with test compounds for 8 h. NO production was measured with the CLSM with excitation and emission wavelengths of 495 and 515 nm, respectively.

### NO Release Measurement *In Vitro* Using Griess Assay

The levels of nitrite were determined by the colorimetric assay using the nitrite colorimetric assay kit (Beyotime, Nanjing, China). Briefly, cells were treated with the indicated concentrations of test compounds, and the nitrite contents of the cell lysates were detected by the Griess assay. The absorbance was read at 540 nm on a spectrophotometer (Smart spec, Bio-Rad). The amount of nitrite in

the lysates was calculated using a  $\text{NaNO}_2$  standard curve in accordance with the manufacturer's instructions.

### MTT Assay

Human TNBC MDA-MB-231 cells, human hepatocarcinomatous HepG2 cells, human breast cancer MCF-7 cells, human cervical carcinoma HeLa cells, human epithelial breast MCF-10A cells, and human fetal hepatocyte L02 cells were plated in a 96-well plate with a concentration of  $10^4$  cells/well and cultured in 37 °C 5%  $\text{CO}_2$  for 24 h. Then, cells were treated in triplicate with or without different concentrations of individual compounds for 72 h. Each concentration was repeated five times in parallel. During the last 4 h culture, the cells were exposed to MTT (5 mg/mL, Sigma-Aldrich), and the resulting formazan crystals were dissolved in DMSO and measured using a spectrophotometer (Tecan) at a test wavelength of 570 nm. Experiments were conducted in triplicate. Inhibition rate (%) =  $[(A_{\text{control}} - A_{\text{treated}})/A_{\text{control}}] \times 100\%$ .

### Pt Cellular Uptake Detection by ICP–MS

The total platinum element ( $^{195}\text{Pt}$ ) including Pt in all valence states in both MDA-MB-231 and MCF-10A cells was detected by ICP–MS. Briefly, when cells grown in a 96-well plate reached 80% confluence, they were washed with PBS before being treated with tested compounds for 12 h or 24 h. Then, the cell lysates were diluted with the ICP–MS diluent (2%  $\text{HNO}_3$  and 0.5% TritonX-100 dissolved in deionized water). The total concentration of  $^{195}\text{Pt}$  was detected with ICP–MS (NexION 2000, PerkinElmer, Shanghai, China), and the total protein concentration in cells was quantified with a BCA protein assay kit (Beyotime, Nanjing, China). The cellular uptake of Pt was calculated as total Pt concentration/total cellular protein concentration.

### Zebrafish Tumor Xenograft Modeling

MDA-MB-231 cells (300–400 cells/embryo) were subcutaneously microinjected into the yolk sac of 48 h post fertilization (hpf) AB wild-type zebrafish embryos. Zebrafish with similar tumor size were randomized divided into several groups, and each group contains at least eight zebrafish.

### NO and Pt Release Measurement in Zebrafish

After establishing the xenograft model, the zebrafish were soaked with vehicle (culture medium) as the vehicle control, and with  $\text{A}_1\text{B}_1$ -BDCN (14.4  $\mu\text{g}/\text{mL}$ ) as the treatment group. The culture medium was changed half every 24 h until photodetection. One day post tumor cell injection (dpi), the drug was administered as described above. The experimental animals (3 dpi) were incubated with RDC1 (20  $\mu\text{M}$ , 3 h) and DAF-FM DA (5  $\mu\text{M}$ , 40 min) 2 days after administration and washed three times with fresh culture medium to remove excess dye. The zebrafish (3 dpi) was then fixed, and the growth state of tumor cells and the release of Pt and NO were recorded using CSLM or stereomicroscopy. At the end of the experiment (3 dpi), the red fluorescence area (representing the proliferation of tumor cells in zebrafish), the intensity of blue fluorescence (representing the release of Pt in the zebrafish), and the intensity of green fluorescence (representing NO release in zebrafish) were analyzed by ImageJ.

### Mouse Tumor Xenograft Model

MDA-MB-231 cells ( $2 \times 10^7/\text{mL}$ ) were subcutaneously injected into the armpit of the BALB/c nude mice. Treatments were initiated when tumors reached a mean group size of approximately 100  $\text{mm}^3$ . Tumor volumes were measured every other day using a Vernier caliper and calculated using the following formula: tumor volume ( $\text{mm}^3$ ) =  $W^2(L/2)$ , where  $W$  = width and  $L$  = length (mm).

### *In Vivo* Fluorescence Imaging

IR-780 is a kind of near-infrared dye for *in vivo* small-animal imaging. IR-780 was loaded into  $\text{A}_1\text{B}_1$ -BDCN to yield IR-780@ $\text{A}_1\text{B}_1$ -BDCN. After the establishment of solid tumor, the mice were randomized and treated intravenously with IR-780 (64.310 mg/L  $\times$  200  $\mu\text{L}$ ) as the vehicle control or IR-780@ $\text{A}_1\text{B}_1$ -BDCN (64.310 mg/L  $\times$  200  $\mu\text{L}$ ) as the experimental group. Drug distribution was evaluated 0, 4, 8, 12,

24, and 48 h after injection with a small-animal live imaging system with excitation and emission wavelengths of 660 and 780 nm, respectively. For evaluation of visceral distribution, the heart, liver, spleen, lung, kidney, and tumor were isolated. Densitometric analysis was implemented to evaluate the drug distribution.

### In Vivo Anticancer Assay

After the establishment of solid tumor, the mice were randomized and treated intravenously with vehicle (saline) as the vehicle control, with A<sub>1</sub>B<sub>1</sub>-BDCN (0.4, 1.2, 3.6 mg/kg) as the low-, middle-, and high-dose groups, or with vehicle (saline) as the vehicle control, with cisplatin (3.6 mg/kg) as the positive control, with A<sub>1</sub>B<sub>1</sub>-BDCN (3.6, 10.8 mg/kg) as the treatment groups. After tumors reached 100–120 mm<sup>3</sup>, test compounds were injected intravenously every other day for consecutive 30 days. The tumor volume and body weight were measured and recorded every day. At the end of treatment, mice were sacrificed and tumors were isolated for taking pictures and weighing.

### Rat Blood Pressure Measurements

Male SD rats were injected i.v. with A<sub>1</sub>B<sub>1</sub>-BDCN or normal saline (blank control) through their tail vein (*n* = 6 per group). Their tail artery blood pressures were measured longitudinally at 0, 2, 4, 9, and 24 h post drug injection using a thermostat noninvasive blood pressure monitor (XH200; Beijing Zhongshi Dichuang Science & Technology Development, Beijing, China).

### Ethics Statement

All animal experiments and animal care were performed in accordance with the guidelines of the Provision and General Recommendation of Chinese Experimental Animals in China. The experimental protocols were approved by the Animal Research and Care Committee of China Pharmaceutical University [No. 2020-07-007].

### Data Analysis

Data are displayed as mean ± SD and analyzed using the software GraphPad Prism 7.0. Differences between multiple groups were analyzed with one-way ANOVA accompanied by Bonferroni's test or the two-way ANOVA accompanied by Bonferroni's test. Differences were recognized to be statistically significant at *P* < 0.05.

## SAFETY STATEMENT

No unexpected or unusually high safety hazards were encountered.

## ASSOCIATED CONTENT

### Supporting Information

The Supporting Information is available free of charge at <https://pubs.acs.org/doi/10.1021/jacsau.2c00390>.

Synthetic routes of ligands for BDCNs; decomposition behaviors of prodrug A or B; characterizations of BDCNs; stability and hemolysis characteristics of A<sub>1</sub>B<sub>1</sub>-BDCN; antiproliferative effects of BDCNs; <sup>195</sup>Pt cellular uptake of A<sub>1</sub>B<sub>1</sub>-BDCN; representative CLSM images of B; structural characterization data of IR-780@A<sub>1</sub>B<sub>1</sub>-BDCN; representative images before treatment with to zebrafish; *in vivo* anticancer effects of treatment with body weight measured and calculated, percent survival rate during the post-treatment period; rat systemic blood pressure detected after treatment with A<sub>1</sub>B<sub>1</sub>-BDCN; concentration of A, B, or Fe in the supernatant or in the BDCN during the synthetic process; and NMR spectra of all new chemical compounds (PDF)

## AUTHOR INFORMATION

### Corresponding Authors

**Ya Ding** – Key Laboratory of Drug Quality Control and Pharmacovigilance, Ministry of Education, China Pharmaceutical University, Nanjing 210009, P. R. China; Email: [dingya@cpu.edu.cn](mailto:dingya@cpu.edu.cn)

**Zhangjian Huang** – State Key Laboratory of Natural Medicines, Jiangsu Key Laboratory of Drug Discovery for Metabolic Diseases, China Pharmaceutical University, Nanjing 210009, P. R. China; [orcid.org/0000-0001-6409-8535](https://orcid.org/0000-0001-6409-8535); Email: [zhangjianhuang@cpu.edu.cn](mailto:zhangjianhuang@cpu.edu.cn)

### Authors

**Jianbing Wu** – State Key Laboratory of Natural Medicines, Jiangsu Key Laboratory of Drug Discovery for Metabolic Diseases, China Pharmaceutical University, Nanjing 210009, P. R. China; [orcid.org/0000-0003-2725-9859](https://orcid.org/0000-0003-2725-9859)

**Yihui Hu** – Key Laboratory of Drug Quality Control and Pharmacovigilance, Ministry of Education, China Pharmaceutical University, Nanjing 210009, P. R. China; Institute for Regenerative Medicine, Shanghai East Hospital, The Institute for Biomedical Engineering & Nano Science, School of Medicine, Tongji University, Shanghai 200092, P. R. China

**Hui Ye** – State Key Laboratory of Natural Medicines, Jiangsu Key Laboratory of Drug Discovery for Metabolic Diseases, China Pharmaceutical University, Nanjing 210009, P. R. China; [orcid.org/0000-0002-1771-7732](https://orcid.org/0000-0002-1771-7732)

**Sheng Zhang** – Key Laboratory of Drug Quality Control and Pharmacovigilance, Ministry of Education, China Pharmaceutical University, Nanjing 210009, P. R. China

**Jie Zhu** – State Key Laboratory of Natural Medicines, Jiangsu Key Laboratory of Drug Discovery for Metabolic Diseases, China Pharmaceutical University, Nanjing 210009, P. R. China

**Duorui Ji** – State Key Laboratory of Natural Medicines, Jiangsu Key Laboratory of Drug Discovery for Metabolic Diseases, China Pharmaceutical University, Nanjing 210009, P. R. China

**Yihua Zhang** – State Key Laboratory of Natural Medicines, Jiangsu Key Laboratory of Drug Discovery for Metabolic Diseases, China Pharmaceutical University, Nanjing 210009, P. R. China; [orcid.org/0000-0003-2378-7064](https://orcid.org/0000-0003-2378-7064)

Complete contact information is available at: <https://pubs.acs.org/10.1021/jacsau.2c00390>

### Author Contributions

J.W. and Y.H. contributed equally to this work. J.W. and Y.H. contributed to synthesis, characterization, solution experiments, and *in vitro* experiments. J.W., Y.H., H.Y., S.Z., J.Z., and D.J. contributed to conducting *in vivo* experiments. J.W. and Y.H. performed statistical analyses; J.W., Y.H., Y.Z., Y.D., and Z.H. contributed to writing, review, and editing; J.W., Y.H., Y.D., and Z.H. received study-enabling funding; Y.D. and Z.H. contributed to initial project conception and supervised the whole project. All authors proof-read, commented on, and approved the final version of the manuscript.

### Notes

The authors declare no competing financial interest.

## ACKNOWLEDGMENTS

This work was supported by grants from the National Natural Science Foundation of China (21977116, 82173681, 31870946, 32271453, 82104004, and 82001953), the Open Project Program of MOE Key Laboratory of Drug Quality Control and Pharmacovigilance (DQCP20/21MS01), open project of State Key Laboratory of Natural Medicines (SKLNMZZ202029), the Funding of Double First-rate discipline construction (CPU2022QZ12 and CPU2022PZQ15), and State Key Laboratory of Pathogenesis, Prevention and Treatment of High Incidence Diseases in Central Asia Fund (SKL-HIDCA-2021-1), and the project funded by China Postdoctoral Science Foundation (2021M693515). We thank Nanjing Xijia Medical Technology Corporation for assistance with the zebrafish assays and thank Dr. Xijing Chen and Shuyue Lei from China Pharmaceutical University for the help with ICP–MS detecting. We specially thank Dr. Binghe Wang from Georgia State University for manuscript wording.

## REFERENCES

- (1) Wei, G.; Wang, Y.; Yang, G.; Wang, Y.; Ju, R. Recent progress in nanomedicine for enhanced cancer chemotherapy. *Theranostics* **2021**, *11*, 6370–6392.
- (2) Poggio, F.; Bruzzone, M.; Ceppi, M.; Pondé, N. F.; La Valle, G.; Del Mastro, L.; de Azambuja, E.; Lambertini, M. Platinum-based neoadjuvant chemotherapy in triple-negative breast cancer: A systematic review and meta-analysis. *Ann. Oncol.* **2018**, *29*, 1497–1508.
- (3) Ghosh, S. Cisplatin: The first metal based anticancer drug. *Bioorg. Chem.* **2019**, *88*, 102925.
- (4) Wang, W.; Zhao, M.; Cui, L.; Ren, Y.; Zhang, J.; Chen, J.; Jia, L.; Zhang, J.; Yang, J.; Chen, G.; Ashby, C. R., Jr.; Wu, C.; Chen, Z. S.; Wang, L. Characterization of a novel HDAC/RXR/HtrA1 signaling axis as a novel target to overcome cisplatin resistance in human non-small cell lung cancer. *Mol. Cancer* **2020**, *19*, 134.
- (5) Li, X.; Hou, Y.; Zhao, J.; Li, J.; Wang, S.; Fang, J. Combination of chemotherapy and oxidative stress to enhance cancer cell apoptosis. *Chem. Sci.* **2020**, *11*, 3215–3222.
- (6) Devaraj, N. K. The future of bioorthogonal chemistry. *ACS Cent. Sci.* **2018**, *4*, 952–959.
- (7) Best, M. D. Click chemistry and bioorthogonal reactions: Unprecedented selectivity in the labeling of biological molecules. *Biochemistry* **2009**, *48*, 6571–6584.
- (8) Baskin, J. M.; Bertozzi, C. R. Bioorthogonal click chemistry: Covalent labeling in living systems. *QSAR Comb. Sci.* **2007**, *26*, 1211–1219.
- (9) Wright, M. H.; Sieber, S. A. Chemical proteomics approaches for identifying the cellular targets of natural products. *Nat. Prod. Rep.* **2016**, *33*, 681–708.
- (10) Thirumurugan, P.; Matosiuk, D.; Jozwiak, K. Click chemistry for drug development and diverse chemical-biology applications. *Chem. Rev.* **2013**, *113*, 4905–4979.
- (11) Wang, W.; Zhang, X.; Huang, R.; Hirschbiegel, C. M.; Wang, H.; Ding, Y.; Rotello, V. M. In situ activation of therapeutics through bioorthogonal catalysis. *Adv. Drug Delivery Rev.* **2021**, *176*, 113893.
- (12) Li, J.; Chen, P. R. Development and application of bond cleavage reactions in bioorthogonal chemistry. *Nat. Chem. Biol.* **2016**, *12*, 129–137.
- (13) Ji, X.; Pan, Z.; Yu, B.; De La Cruz, L. K.; Zheng, Y.; Ke, B.; Wang, B. Click and release: Bioorthogonal approaches to “on-demand” activation of prodrugs. *Chem. Soc. Rev.* **2019**, *48*, 1077–1094.
- (14) Dong, Y.; Tu, Y.; Wang, K.; Xu, C.; Yuan, Y.; Wang, J. A general strategy for macrotheranostic prodrug activation: Synergy between the acidic tumor microenvironment and bioorthogonal chemistry. *Angew. Chem., Int. Ed.* **2020**, *59*, 7168–7172.
- (15) Versteegen, R. M.; Rossin, R.; ten Hoeve, W.; Janssen, H. M.; Robillard, M. S. Click to release: Instantaneous doxorubicin elimination upon tetrazine ligation. *Angew. Chem., Int. Ed.* **2013**, *52*, 14112–14116.
- (16) Yao, Q.; Lin, F.; Fan, X.; Wang, Y.; Liu, Y.; Liu, Z.; Jiang, X.; Chen, P. R.; Gao, Y. Synergistic enzymatic and bioorthogonal reactions for selective prodrug activation in living systems. *Nat. Commun.* **2018**, *9*, 5032.
- (17) Sancho-Albero, M.; Rubio-Ruiz, B.; Pérez-López, A. M.; Sebastián, V.; Martín-Duque, P.; Arruebo, M.; Santamaría, J.; Unciti-Broceta, A. Cancer-derived exosomes loaded with ultrathin palladium nanosheets for targeted bioorthogonal catalysis. *Nat. Catal.* **2019**, *2*, 864–872.
- (18) Zheng, Y.; Ji, X.; Yu, B.; Ji, K.; Gallo, D.; Cszimadia, E.; Zhu, M.; Choudhury, M. R.; De La Cruz, L. K. C.; Chittavong, V.; Pan, Z.; Yuan, Z.; Otterbein, L. E.; Wang, B. Enrichment-triggered prodrug activation demonstrated through mitochondria-targeted delivery of doxorubicin and carbon monoxide. *Nat. Chem.* **2018**, *10*, 787–794.
- (19) Wang, J.; Liu, Y.; Liu, Y.; Zheng, S.; Wang, X.; Zhao, J.; Yang, F.; Zhang, G.; Wang, C.; Chen, P. R. Time-resolved protein activation by proximal decaging in living systems. *Nature* **2019**, *569*, 509–513.
- (20) Li, J.; Yu, J.; Zhao, J.; Wang, J.; Zheng, S.; Lin, S.; Chen, L.; Yang, M.; Jia, S.; Zhang, X.; Chen, P. R. Palladium-triggered deprotection chemistry for protein activation in living cells. *Nat. Chem.* **2014**, *6*, 352–361.
- (21) Huang, Z.; Fu, J.; Zhang, Y. Nitric oxide donor-based cancer therapy: Advances and prospects. *J. Med. Chem.* **2017**, *60*, 7617–7635.
- (22) Hu, Y.; Lv, T.; Ma, Y.; Xu, J.; Zhang, Y.; Hou, Y.; Huang, Z.; Ding, Y. Nanoscale coordination polymers for synergistic NO and chemodynamic therapy of liver cancer. *Nano Lett.* **2019**, *19*, 2731–2738.
- (23) Klein, A. V.; Hambley, T. W. Platinum drug distribution in cancer cells and tumors. *Chem. Rev.* **2009**, *109*, 4911–4920.
- (24) Rieter, W. J.; Pott, K. M.; Taylor, K. M. L.; Lin, W. Nanoscale coordination polymers for platinum-based anticancer drug delivery. *J. Am. Chem. Soc.* **2008**, *130*, 11584–11585.
- (25) Poon, C.; Duan, X.; Chan, C.; Han, W.; Lin, W. Nanoscale coordination polymers codeliver carboplatin and gemcitabine for highly effective treatment of platinum-resistant ovarian cancer. *Mol. Pharm.* **2016**, *13*, 3665–3675.
- (26) He, C.; Poon, C.; Chan, C.; Yamada, S. D.; Lin, W. Nanoscale coordination polymers codeliver chemotherapeutics and siRNAs to eradicate tumors of cisplatin-resistant ovarian cancer. *J. Am. Chem. Soc.* **2016**, *138*, 6010–6019.
- (27) Sun, T.; Lv, T.; Wu, J.; Zhu, M.; Fei, Y.; Zhu, J.; Zhang, Y.; Huang, Z. General strategy for integrated bioorthogonal prodrugs: Pt(II)-triggered depropargylation enables controllable drug activation in vivo. *J. Med. Chem.* **2020**, *63*, 13899–13912.
- (28) Scarano, W.; de Souza, P.; Stenzel, M. H. Dual-drug delivery of curcumin and platinum drugs in polymeric micelles enhances the synergistic effects: A double act for the treatment of multidrug-resistant cancer. *Biomater. Sci.* **2015**, *3*, 163–174.
- (29) Weaver, E. L.; Bose, R. N. Platinum(II) catalysis and radical intervention in reductions of platinum(IV) antitumor drugs by ascorbic acid. *J. Inorg. Biochem.* **2003**, *95*, 231–239.
- (30) Chen, C. K.; Zhang, J. Z.; Aitken, J. B.; Hambley, T. W. Influence of equatorial and axial carboxylato ligands on the kinetic inertness of platinum(IV) complexes in the presence of ascorbate and cysteine and within DLD-1 cancer cells. *J. Med. Chem.* **2013**, *56*, 8757–8764.
- (31) Dabbish, E.; Ponte, F.; Russo, N.; Sicilia, E. Antitumor platinum(IV) prodrugs: A systematic computational exploration of their reduction mechanism by L-ascorbic acid. *Inorg. Chem.* **2019**, *58*, 3851–3860.
- (32) Bredt, D. S.; Snyder, S. H. Nitric oxide: A physiologic messenger molecule. *Annu. Rev. Biochem.* **1994**, *63*, 175–195.

(33) Kinnear, C.; Moore, T. L.; Rodriguez-Lorenzo, L.; Rothen-Rutishauser, B.; Petri-Fink, A. Form follows function: Nanoparticle shape and its implications for nanomedicine. *Chem. Rev.* **2017**, *117*, 11476–11521.

(34) Zhang, S.; Gao, H.; Bao, G. Physical principles of nanoparticle cellular endocytosis. *ACS Nano* **2015**, *9*, 8655–8671.

(35) Lee, U. Y.; Youn, Y. S.; Park, J.; Lee, E. S. Y-shaped ligand-driven gold nanoparticles for highly efficient tumoral uptake and photothermal ablation. *ACS Nano* **2014**, *8*, 12858–12865.

(36) Kolesnik, B.; Palten, K.; Schrammel, A.; Stessel, H.; Schmidt, K.; Mayer, B.; Gorren, A. C. Efficient nitrosation of glutathione by nitric oxide. *Free Radic. Biol. Med.* **2013**, *63*, 51–64.

(37) Hong, R.; Han, G.; Fernández, J. M.; Kim, B. J.; Forbes, N. S.; Rotello, V. M. Glutathione-mediated delivery and release using monolayer protected nanoparticle carriers. *J. Am. Chem. Soc.* **2006**, *128*, 1078–1079.

(38) Ong, J. X.; Lim, C. S. Q.; Le, H. V.; Ang, W. H. A ratiometric fluorescent probe for cisplatin: Investigating the intracellular reduction of platinum(IV) prodrug complexes. *Angew. Chem., Int. Ed.* **2019**, *58*, 164–167.

(39) Kojima, H.; Urano, Y.; Kikuchi, K.; Higuchi, T.; Hirata, Y.; Nagano, T. Fluorescent indicators for imaging nitric oxide production. *Angew. Chem., Int. Ed.* **1999**, *38*, 3209–3212.

(40) Yue, C.; Liu, P.; Zheng, M.; Zhao, P.; Wang, Y.; Ma, Y.; Cai, L. Ir-780 dye loaded tumor targeting theranostic nanoparticles for nir imaging and photothermal therapy. *Biomaterials* **2013**, *34*, 6853–6861.

(41) Pignatello, J. J.; Oliveros, E.; MacKay, A. Advanced oxidation processes for organic contaminant destruction based on the fenton reaction and related chemistry. *Crit. Rev. Environ. Sci. Technol.* **2006**, *36*, 1–84.

(42) Ellis, L.; Er, H.; Hambley, T. The influence of the axial ligands of a series of platinum(IV) anti-cancer complexes on their reduction to Platinum(II) and reaction with DNA. *Aust. J. Chem.* **1995**, *48*, 793–806.

(43) Xue, R.; Wu, J.; Luo, X.; Gong, Y.; Huang, Y.; Shen, X.; Zhang, H.; Zhang, Y.; Huang, Z. Design, synthesis, and evaluation of diazeniumdiolate-based DNA cross-linking agents activatable by glutathione S-transferase. *Org. Lett.* **2016**, *18*, 5196–5199.

#### NOTE ADDED AFTER ASAP PUBLICATION

This article was published ASAP on October 5, 2022. Text in the *In Vivo* Anticancer Assay section has been updated and the corrected version was reposted on October 6, 2022.